Faculty and Researchers   Faculty and Researchers' Publications

2020-06-20

Enhancement of electrical conductivity of carbon nanotube sheets through copper addition using reduction expansion synthesis

Earp, Brian; Aceves, Patrick; Dunn, Durward; Phillips, Jonathan; Agrawal, Richa; De Rosa, Igor; Xin, Wenbo; Ansell, Troy; Luhrs, Claudia

Elsevier

This publication is a work of the U.S. Government as defined in Title 17, United

Enhancement of electrical conductivity of carbon nanotube sheets through copper addition using reduction expansion synthesis

Brian Earp[a,*], Durward Dunn[a], Jonathan Phillips[b], Richa Agrawal[a], Troy Ansell[a], Patrick Aceves[c], Igor De Rosa[d], Wenbo Xin[d], Claudia Luhrs[a]

[a] Department of Mechanical and Aerospace Engineering, Naval Postgraduate School, Monterey, CA 93943, USA
[b] Energy Academic Group, Naval Postgraduate School, Monterey, CA 93943, USA
[c] NREIP Summer 2019 Intern at Naval Postgraduate School, Monterey, CA 93943 USA
[d] Craytex LLC, 621 Hindry Ave., Inglewood, CA 90301, USA and Department of Materials Science and Engineering, University of California Los Angeles, 410 Westwood Plaza, Los Angeles, California 90095, USA

ABSTRACT

The ability to translate the high electrical conductivity of individual carbon nanotubes to bulk carbon nanotube materials has proven challenging. In this work, we present the use of reduction expansion synthesis to attach copper nanoparticles to the surface of tubes within carbon nanotube sheets. Those metallic particulates serve as a link between the tube strands in the carbon nanotube network and promote an increase in electrical conductivity. The reduction expansion synthesis process included the introduction of copper salts into the carbon nanotube structure and thermal treatment of the sheets in the presence of urea, under inert atmospheres. As a result, through the reduction process promoted by the urea decomposition byproducts, copper nanoparticles directly nucleate on the nanotube surface. The enhanced conductive nature of the Cu-carbon nanotube sheets observed establishes reduction expansion synthesis as an inexpensive, rapid and scalable alternative to increase the electrical conductivity of bulk carbon nanotube materials.

1. Introduction

While the electrical conductive capabilities of CNTs have long been recognized following their formal discovery in 1991 [1], translating the individual nanotube conductivity to high levels of conductivity in various bulk CNT forms (yarns, sheets, composites, etc.) has proven challenging [2]. CNTs have routinely been investigated as a filler material in composites [3–5] and have been processed in order to create CNT yarns and sheets with desirable properties [2]. Since the 1990s, CNT production has significantly increased [6], however the electrical, mechanical, and thermal properties of bulk CNT materials do not yet align with the properties of individual CNTs [6,7]. For example, the electrical conductivity of single-walled CNTs (SWCNT) has been reported to be on the order of 10^2 to 10^6 S/cm, multi-walled CNTs (MWCNT) are 10^3 to 10^5 S/cm [8] and CNT fibers have conductivities that could vary in orders of magnitude, ranging from 10 to 67,000 S/cm [2]. The potential for the use of CNTs in electrical applications such as electrostatic discharge [3], electromagnetic interference prevention [3], and actual wiring [2] requires higher conductivities than the ones observed experimentally in extended structures such as sheets, ropes

and wires, thus, efforts focused on improving the electrical performance are of vital importance for the applicability of these materials.

Improving and/or tailoring of the electrical conductivity of CNTs is not a novel idea and multiple efforts to achieve higher performance have been reported, most of them have focused on the doping of CNTs [9,10]. Doping efforts have been achieved through the intercalation of elements such as potassium, iodine, lithium, metallic chlorides, halogens, and nitrogen in both, SWCNTs and MWCNTs [9,11–13]. Significant work with nitrogen doping of CNTs has been done though a substitutional process to form heteronanotubes and through endohedral doping where CNTs are filled with the dopant [12]. Other efforts to improve electrical conductivity have been focused on direct modification of individual CNTs, i.e. dispersed in solution [10] or during their CVD growth process. Introduction of secondary phases has been accomplished by the precipitation of gold nanoparticles onto CNTs [10]. However, there are only a few reports in regard to the introduction of secondary phases or dopants into CNTs once that those are part of a yarn, sheet, wire, or composite. Zhao et al reported the doping of CNT sheets and cables with iodine, which resulted in a reduction of double walled CNT cables' resistivity from an undoped value of $\sim 5 \times 10^{-7}$

Ohm-m to a doped value of $\sim 1.5 \times 10^{-7}$ Ohm-m (electrical conductivity changed from $\sim 2 \times 10^6$ S/m to $\sim 6.7 \times 10^6$ S/m) [14]. Doping CNT sheets and yarns with iodine monobromide by Bucossi et al. resulted in electrical conductivity improving from 1.0×10^5 S/m to 0.85×10^6 S/m for CNT sheets and from 1.0×10^5 S/m to 14×10^5 S/m for CNT yarns [15]. Additionally, densification of CNT wires via tungsten carbide drawing and subsequent doping by exposure to a potassium tetrabromoaurate solution, a bulk electrical conductivity of 1.3×10^6 S/m (approximately one order of magnitude increase from undoped to doped) was obtained by Alvarenga, et al. [16]. Recently, efforts to create copper-CNT hybrids using CVD by Leggiero et al. resulted in conductivities of 28.1×10^6 S/m, an increase from 4.94×10^4 S/m, however, with a relatively high copper weight concentration of 94.2 % [17]. Herein, the Reduction Expansion Synthesis (RES) process, a relatively new technique, is used to improve the overall electrical conductivity of CNT sheets using inexpensive precursors by a process that barely changes the sample weight, only takes a minimal amount of time per batch, and has great potential for scalability and adoption.

The unique RES process, first described in 2010 [18,19], requires precursors to be combined with a reducing agent, such as urea, and heated above the decomposition temperature of the reducing agent in an inert atmosphere which results in the release of reducing gaseous species. The individual steps that urea undergoes during its decomposition have been highlighted elsewhere [18]. As described by Zea et al. [19], the mechanism for the RES process for metal reduction transforms the precursors to zero-valence metals and could render finely divided particulates.

Since the identification of the RES process as an effective tool to generate reduced products, the method has been used in several applications. Specifically, the RES process has been used to produce graphene from graphite oxide with urea used as an expansion-reduction agent [18,20]. This technique has also been adapted to synthesize nano and micro-scale metallic particles through an aerosol process by Soliman et al. [21] and to create submicron and nanometal particles through heating metal nitrates and urea [19]. A consolidated description of the impact of precursors, gas flow rates, and temperatures on the RES process was provided by Luhrs et al. [22] during the reduction of metal oxides and hydroxides. The RES process has also been used as a means to promote and manage nitrogen doping in graphene both using a standard RES process [23] and through use of a combined microwave plasma and RES process [24].

Other efforts have been made to use urea as a reducing agent for the development of graphene nanosheets to be used for transparent conducting films [25] and the synthesis of nitrogen-doped graphene nanosheets [26]. Some of the most recent work using the RES process has branched out into unique applications to include using the RES process to produce a micron scale chrome coating on metals [27], using the process to create tin/carbon battery electrodes [28], and using the process to create platinum nanorafts on an Mo_2C substrate for electrocatalysis [29]. The development and use of the RES process has prompted the consideration of other applications for this novel and relatively straightforward process for efficiently and effectively reducing metal precursors to zero-valent metallic particles.

2. Experimental methods

2.1. Materials

The CNT samples employed for this work were CNT sheets manufactured by Nanocomp Technologies, Inc, A Huntsman Company (New Hampshire), using an iron catalyst in a CVD process. The sheets consisted of bundles of CNTs that were on the order of hundreds of microns in width and up to millimeters in length [30] with iron contents in the order of 22 % by wt. A second type of CNT sheets, produced by removing iron from the former CNT type to achieve approximately 3% by wt of Fe, were provided by Craytex LLC. A proprietary process involving energetic gas was employed to clean the polymeric amorphous carbon and excess iron catalyst from mass-produced CNT sheets. Thus, two types of CNT sheets of varying iron catalyst amounts (here denominated 'high Fe' and 'low Fe') were analyzed. Raw materials used for the RES process included copper (II) nitrite trihydrate ($Cu_2(NO_3)_2.3H_2O$), urea (CH_4N_2O), and ethyl alcohol, all obtained from Sigma Aldrich (St. Louis, Missouri).

2.2. Fabrication protocols

Fabrication involved RES processing of i) as received low Fe CNT sheets, ii) activated low Fe CNT sheets, and iii) as received high Fe CNT sheets. Additionally, for comparison purposes, low Fe CNT sheets were sputter coated with Pt-Pd and conductivity values from a sheet of Cu foil were obtained. A summary of samples is included in Table 1 below.

The addition of a second phase (copper) to CNT sheets was accomplished through the RES-Cu process as described below. A sample of the CNT sheet was cut into a small strip, weighed, and measured in order to determine the amount of copper salts (copper (II) nitrite trihydrate) to be used during the RES process based on a molar mass calculation and target copper concentrations of 3%, 10 %, and 15 %. The copper salts were then dissolved in ethyl alcohol and the solution was applied to both sides of the CNT sheet and allowed to air dry. In an attempt to ensure a relatively even distribution of copper across the sheet, the solution was carefully spread over the length of the sheet using a dropper. Following drying of the CNT sheet and copper solution, the necessary amount of urea was calculated, crushed using a mortar and pestle, and placed in the bottom of an alumina boat. The amount of urea used was based on a copper nitrate:urea 1:5 ratio. A sheet of grafoil, perforated with small holes, was placed over the urea in order to allow byproducts from the urea decomposition to diffuse through the grafoil during heating and be flushed out via an inert gas flow of argon. The CNT sheet was then placed on top of the grafoil and the entire boat assembly (Fig. 1) was placed in a quartz tube. The quartz tube was flushed with argon for approximately one hour and then placed in a tube furnace (Thermo Scientific Lindberg/Blue M model TF55035A-1) for 10 min at 800 degrees C. Following thermal treatment, the sample was removed from the furnace and allowed to cool before further analysis.

Some of the low Fe CNT sheets were subjected to an activation process that consisted of heating the CNT sheets in an open ended quartz tube, thus exposed to air, and raising temperature to 500 degrees Celsius over 30 min, holding at 500 degrees Celsius for two hours and then cooling to room temperature. The activation process was used in

Table 1
Summary of Samples Analyzed.

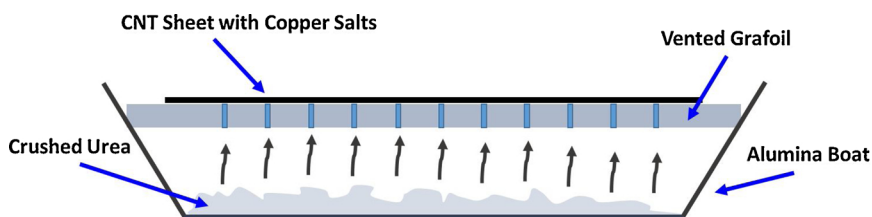| Sample	RES Process	Details
High Fe CNT Sheet (As-Received)	Yes	0% Cu, 3% Cu, 10 % Cu, 15 % Cu
Low Fe CNT Sheet (As-Received)	Yes	0% Cu, 3% Cu, 10 % Cu, 15 % Cu
Low Fe CNT Sheet (Activated)	Yes	0% Cu, 3% Cu, 10 % Cu, 15 % Cu
Low Fe CNT Sheet (Pt-Pd Sputtered)	No	3 nm Pt-Pd, 10 nm Pt-Pd
Cu Foil	No	As-Received

an attempt to increase the number oxygen species and dangling bonds in the CNTs surface to promote the attachment of copper particles to the CNTs.

Some as-received low Fe CNT sheets were separately coated with thin layers of Pt-Pd via sputter coating (Pt-Pd 80/20 target) to determine the impact on electrical conductivity and provide another comparison point. Samples were coated with two different Pt-Pd coating thicknesses (3 nm and 10 nm) using a Cressington Sputter Coater 208HR.

2.3. Characterization techniques

A Scanning electron microscope (SEM) was used to analyze the CNT sheet microstructure and Cu distribution. A Zeiss Neon 40 (Carl Zeiss Inc., Thornwood, NY, USA) field emission SEM operating between 1–20 kV and coupled with an EDAX Energy Dispersive X-ray Microanalysis system with Analytical Drift Detector was used for analysis. High resolution Transmission electron microscopy (HRTEM) images to support CNT sheet microstructural analysis before and after copper addition were obtained using an FEI Titan $80-300$ kV scanning TEM (STEM) at an accelerating voltage of 300 kV and an FEI Tecnai Osiris STEM operating at 200 kV, respectively. Raman scattering measurements of CNT sheets were performed using a Renishaw In-Via Raman spectrometer. The employed laser wavelength and the power were 785 nm and 0.25 mW, respectively. During measurements, an objective lens magnification of 50x and a grating spacing of 1200 L/mm were used. Spectral resolution in data is 1 cm^{-1}. In order to thermally characterize samples, a Netzsch STA 449 Jupiter F3 simultaneous thermal analyzer was used primarily to determine the amount of iron catalyst present in as-received CNT sheet samples. The samples were heated at a rate of 20 degrees Celsius per minute from 25 degrees to 900 degrees in a 20 % O_2 and 80 % N_2 atmosphere.

2.4. Electrical resistivity measurements

After completion of the RES-Cu process, electrical resistivity measurements were performed using a four-point probe with sample thickness determined using digital calipers and a thickness gauge. Electrical resistivity measurements were conducted using a Lucas Labs Pro4 four-point probe in accordance to ASTM Standard F84-99 (ASTM F84-99). Testing with the four-point probe included taking measurements in an X-Z direction with the probes aligned in the same direction as the CNT sheet (Fig. 2). Electrical resistivity measurements were also performed on the sputter coated low Fe CNT sheets and a 0.5 mm thick sheet of copper foil in order to compare with CNT sheets that underwent RES-Cu process. All resistivity measurements were converted to conductivity values to support comparison with values reported in other references.

3. Results and discussion

3.1. As-received CNT sheet characterization

The CNT sheets received from both Nanocomp Technologies, Inc. and Craytex LLC consisted of bundled CNTs with iron catalyst particles remaining from the production process. The iron catalyst percentages
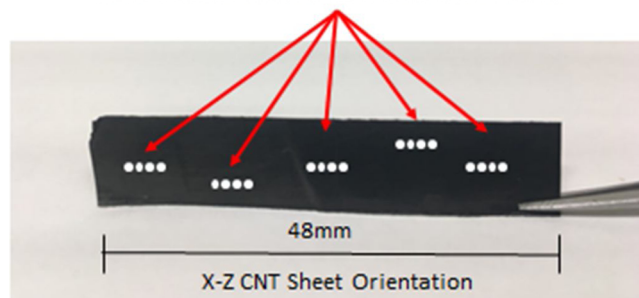

Fig. 2. CNT Sheet Orientation During Four Point Probe Measurements.

were determined via thermogravimetric analysis using oxygen containing atmospheres. Iron catalyst percentages were determined to vary between $\sim 2.5-5\%$ wt based on multiple analyses from different sample locations on the low Fe CNT sheets and were approximately ~ 22 % wt for the high Fe CNT sheets.

CNT sheets were analyzed using SEM and TEM in order to gain an understanding of the 'as received' sheets microstructures for the high and low Fe CNT sheets. Fig. 3 shows an SEM image of an as-received high Fe CNT sheet. At low magnifications (Fig. 3(a)), the iron catalyst particles are not easily distinguished from the CNTs, however at higher magnifications iron catalyst particles are clearly evident throughout the CNT sheet (Fig. 3(b)). The iron particulates consist of nearly spherical shapes for those of approximately 5 nm and irregular shapes for the ones in the 100 nm range. The lower magnification image shows a certain level of alignment of the CNT bundles in the direction of the CNT sheet.

HRTEM shows nanoparticles of metallic catalyst (Fe) encapsulated in few-layered graphitic shells or amorphous carbon in as-received high Fe CNT sheet (Fig. 4(a) and (b)) and mostly empty graphitic shells in the low Fe CNT sheets (Fig. 4(c) and (d)).

Raman spectroscopy was performed in order to evaluate the degree of crystallinity of the CNT sheets. Fig. 5 compares the high-frequency Raman spectra of the high Fe CNT sheet (solid blue) and low Fe CNT sheet (solid red). The curves show the two characteristic peaks of multi-walled CNTs: the G-band at 1580 cm^{-1} and the D-band at 1308 cm^{-1} [31]. The G-band is indicative of well-ordered structure associated with sp^2 carbon atoms in the CNT sidewalls while the D-band corresponds to either sp^3 carbon atoms at defect sites in the CNT sidewalls or amorphous carbon [32]. While no noticeable shift in frequency of the two peaks before and after cleaning was observed, the analysis of the intensity of D and G band shows that the intensity ratio (I_D/I_G) value drastically decreased from 0.56 (high Fe CNT) to 0.16 (low Fe CNT (Fig. 5), indicating that after the treatment the degree of crystallinity is increased [33].

3.2. CNT sheet microstructure following RES process

SEM and TEM were also used to compare pre and post-RES-Cu process CNT sheet samples to observe and analyze the morphology and amount of copper deposited on the CNT sheets. Following the RES-Cu process, designed to generate target copper concentrations by weight of 0%, 3%, 10 %, and 15 %, SEM images showed the size of copper
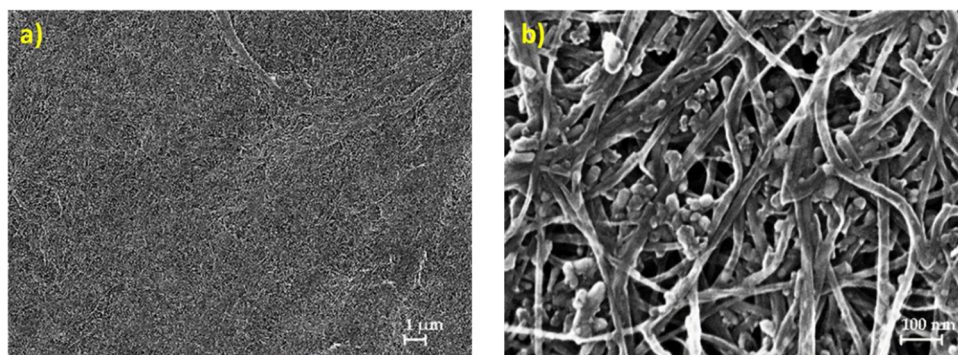
Fig. 3. SEM Images of the As-Received CNT Sheet. a) Taken at 5,000x Magnification Showing the Overall Sheet Features and b) 100,000x Magnification Highlighting Iron Particles within the CNT Bundles.

particle agglomerates, increases with increasing copper concentration (Fig. 6). At a concentration of 3% copper, the copper particle sizes range from approximately 20 nm–150 nm with a relatively even dispersion on the CNT sheet. At a concentration of 10 % copper, the smaller copper particles are relatively homogenously dispersed across the CNT sheet, however, some of the particles agglomerated into larger particles with sizes up to about 400 nm. At a concentration of 15 % copper, more significant agglomeration occurred with combined particles as large as ~800 nm and the dispersion of the smallest copper particles appeared more varied on the CNT sheet.

Small particles are assessed to have formed at active sites, perhaps defects. As the copper concentration increases, these sites become saturated and no additional metal can attach to the carbon. Thus, additional metal atoms only weakly attach to the "basal plane" sites on the CNT probably via Van der Waals forces. Weakly bound metal atoms migrate rapidly, interacting with other weakly bound metal atoms or clusters of atoms. This leads to particle growth via agglomeration as

discussed above. The same model of metal particle growth on carbon, the so-called weak metal support interaction (WMSI) model was postulated earlier to explain platinum and palladium growth on carbon [34,35] and discussed in terms of CNT production with Fe/Al$_2$O$_3$ and Fe-Ni/Al$_2$O$_3$ catalysts [36].

The coagulation of copper particles and formation of agglomerates can be related to the statistical model proposed by Smoluchowski in 1916 [37] and further expanded upon by others to explain particle dynamics during a period of nucleation, coagulation, and surface growth occurring at the same time [38,39]. Similar discussion of particle aggregation is routinely discussed when describing the formation of soot [40,41]. Fig. 6 illustrates this increased agglomeration as copper percentage is increased during the RES process for a high iron content non-activated CNT sheet. At higher magnifications, the sizes of the metallic particles can be more clearly seen.

Fig. 7 shows SEM images at diverse magnifications (a and b) and EDS analysis (c) of a CNT sheet with 10 % copper. In those particular
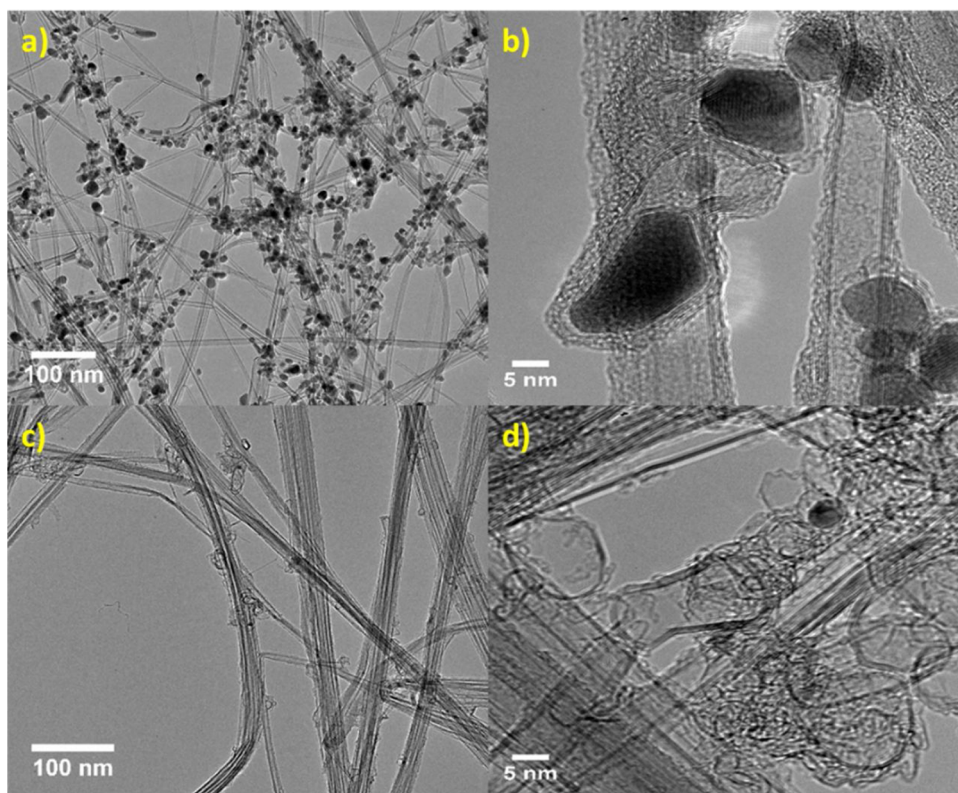

Fig. 4. HR-TEM Images of As-Received High Fe CNTs at a) Low and b) High Magnification Showing Significant Number of Fe Catalyst Particles Encapsulated in Graphitic Shells and of Low Fe CNTs at c) Low and d) High Magnification Showing Empty Graphitic Carbon Shells from which Fe was Removed.
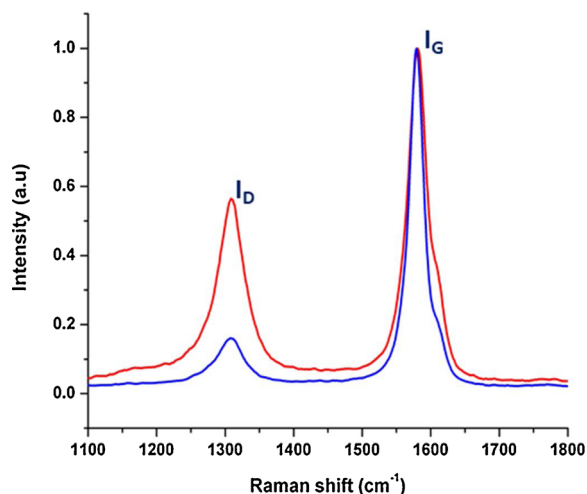
Fig. 5. Comparison of Raman Spectra of CNT sheets Before (red line) and After Cleaning (blue line).

locations, the majority of the individual CNTs and CNT bundles can be seen to have a horizontal alignment with clear gaps between the CNT structures, which provide optimal locations for the copper particles to nucleate and attach to the CNTs. The copper particles provide a connection between adjacent CNTs and are assessed to be the reason for improved electrical conductivity after copper is added to the CNT sheets. Particles of approximately 25–300 nm size can be clearly seen providing a bridge on top (a) or in between (b) nearby CNTs. Energy dispersive spectroscopy (EDS) of the area in Fig. 7(a), consistent with other areas analyzed, identifies C, Cu and S as elemental constituents of the sample. The carbon signal originates from the CNTs, copper from the particulates added, and sulfur from the CNT sheet fabrication process environment.

TEM analysis was conducted on CNT sheet samples that had been subjected to the RES-Cu process in order to identify the areas of interaction between copper particles and CNTs. Fig. 8(a) shows a TEM

image of an activated low Fe content 10 % copper sample showing a copper particle attached to CNTs and providing a bridge between CNTs similar to that seen in the SEM image above. Fig. 8(b) presents a HAADF image and Fig. 8(c–e) are X-Ray EDS microanalysis maps used to positively identify the particle as copper and the location of the carbon nanotubes and iron catalyst particles that are present in nearby locations. Fig. 8(a) clearly supports the theory that copper particles are providing connections between adjacent CNTs and improving electrical conductivity. Given the presence of a graphitic shell surrounding some of the Cu particles, it is believed that, at least to some extent, the forces keeping the Cu and CNT bundles together include van der Waals interactions.

3.3. Factors that impact CNT sheet electrical conductivity

CNT sheet electrical conductivity for low and high Fe content samples was clearly impacted by the presence of metallic particles (iron catalyst and deposited copper particles) and the activation process employed in an attempt to create more dangling bonds in the CNT sheet. A detailed description of the specific factors is provided below.

3.3.1. Metal particles (Fe catalyst and Cu as secondary phase)

The electrical conductivity for CNT sheets increased with copper additions of 3%, 10 %, and 15 % wt regardless of activation status or Fe content. For non-activated low Fe CNT sheet, a 10 % copper content showed the most significant impact with an approximately 3.4X magnitude increase from the as-received CNT sheet. For activated low Fe CNT sheet with a 10 % copper content, the increase was approximately 4.0X. For the non-activated high Fe CNT sheets, the increase was less significant with an approximate 1.7X increase for 10 % copper content. While conductivity values at copper concentrations of 15 % are still higher than 0% copper samples, the increase in conductivity is not as great as the 10 % copper sample. Fig. 9(a) illustrates observed values for the high Fe CNT sheet and presents a maximum magnitude conductivity value at 10 % copper. It is worth noting that each measurement presented in Fig. 9 represents the average of five measurement locations on each sample. As previously discussed and as can be seen in
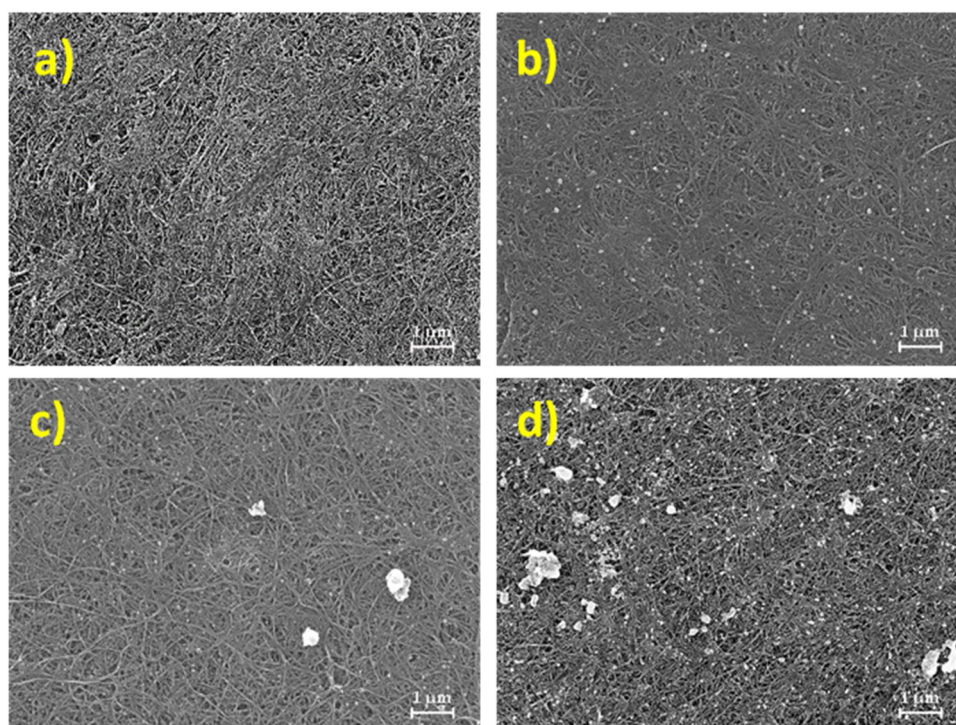

Fig. 6. SEM Images Taken at 10,000x Magnification of CNT Sheets a) 0% Copper, b) 3% Copper, c) 10 % Copper, and d) 15 % Copper.
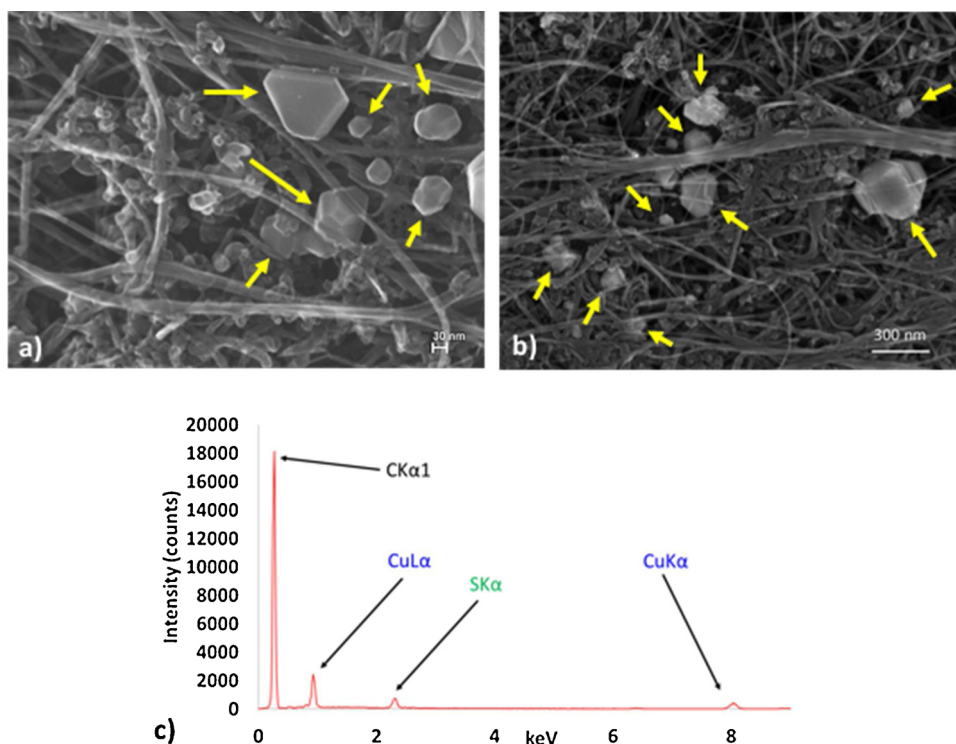
Fig. 7. SEM Images Showing Copper Particles Bridging a) the Top Layer or b) Internal Regions of CNTs in Specimen with 10 % Copper. c) EDS Analysis of the Area Presented in a).

Fig. 6, at higher concentrations, the copper particles seem to agglomerate more, resulting in less copper particles throughout the CNT sheet to support bridging between CNTs. As a result, the improved conductivity tends to drop off at higher copper concentration levels.

Fig. 9(b) shows normalized conductivity values of the low and high Fe CNT sheets for activated (low Fe) and non-activated (low and high Fe) samples with varying amounts of copper including the as-received condition, 3% copper, 10 % copper, and 15 % copper. The as-received CNT sheet conditions for low and high Fe content were used to normalize the values for conductivity. Absolute conductivity values of the high Fe samples (Fig. 9(a)) are higher than the absolute conductivity values of low Fe samples which is consistent with a CNT composite study that show higher conductivities for samples with higher catalyst percentages [42]. It is believed that the magnitude increase in conductivity for the low Fe samples is higher than for the high Fe samples because the additional iron in the high Fe samples resulted in less locations for the copper particles to deposit onto the CNT active sites.

3.3.2. CNT sheet activation

As shown in Fig. 9(b), the activation of the low Fe CNT sheets resulted in an improvement of conductivity for 3% and 10 % copper concentrations. Activated carbon structures are known for their high porosity and large surface area that is a result of defects and disorder from the activation process [43,44]. The improved performance of the activated CNT sheets is assessed to be due to the creation of more dangling bonds during the activation process, which provide a greater likelihood for copper carbon attachment during the RES process.

While other work, using both a two-step sensitization and chemical activation process and a single step chemical activation process, demonstrated the ability for coating of CNTs with copper and nickel [45], this basic activation presented herein and subsequent RES process provides a different method for attaching copper particles to CNTs.

3.3.3. Conductivity comparison between Cu-CNT, sputtered Pt/Pd CNT and bare copper foil

Sputter coating a 3 nm and 10 nm Pt-Pd layer on the CNT sheets improved conductivity from 3.1×10^4 S/m to 6.1×10^4 S/m and 6.8×10^4 S/m, respectively, whereas a copper concentration of 10 % using the RES process improved conductivity up to 5.4×10^4 S/m for a high Fe CNT sheet. The conductivity values for the Pt-Pd coating on the CNT sheets are below nominal bulk conductivity values of Platinum and Palladium (9.4×10^6 S/m and 1.0×10^7 S/m, respectively), however this is likely due to the thin coating layers. The improvement in CNT sheet conductivity via copper addition using the RES process is comparable to the improvement achieved by sputter coating various thicknesses of Pt-Pd onto the CNT sheet. The Pt-Pd coating is a continuous layer on top of the CNT sheet that is not well adhered and is highly susceptible to delamination. Additionally, the use of Pt-Pd sputter coating leads to increased weight and cost that would be undesirable in most applications. A copper foil sheet with a measured conductivity of 1.0×10^7 S/m represents a much more conductive material and was employed for reference. While the electrical conductivity of the CNT sheets is not yet on the same order of magnitude as measured copper foil, the RES process clearly improved conductivity and this method is a step towards bulk CNT materials being able to obtain the electrically conductive properties of their individual CNTs. A comparison of CNT sheets with copper deposition, CNT sheets sputter coated with Pt-Pd, and 0.5 mm thick copper foil is provided in Fig. 10.

3.4. RES as unique method for addition of second phase metal to CNT sheets

Previous work by others has focused on the addition of second phases to CNTs by methods such as doping [9,10] and less commonly on the addition of metals to CNT sheets. The RES process provides an effective method to add a second phase (copper metal) to CNT sheets, leading to relative changes in conductivity (1.4X to 4.0X increase) approaching increases seen in monobromide doping of CNT sheets (8.5X)
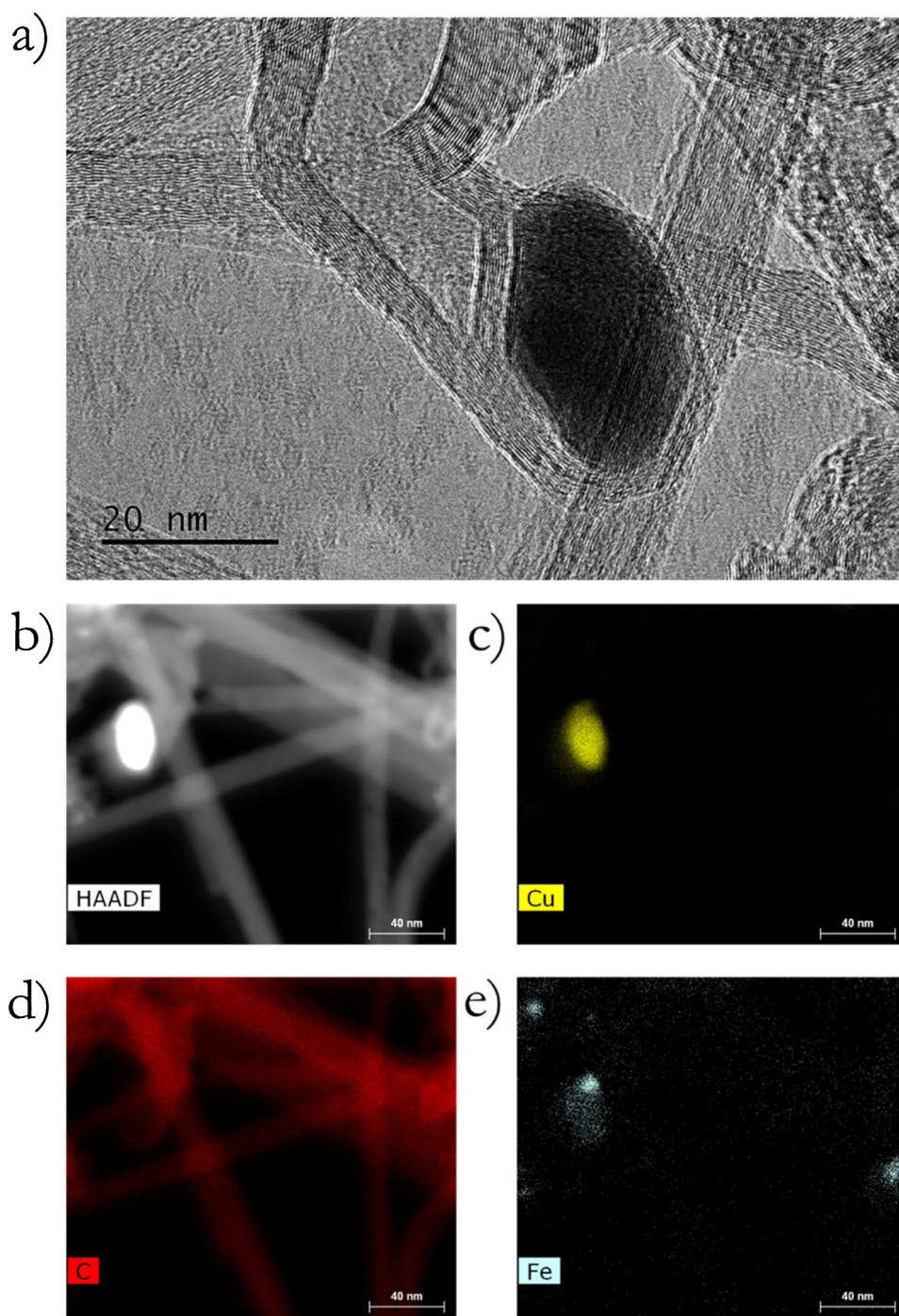
Fig. 8. a) TEM Image Showing Copper-CNT Interaction in CNT Sheet with 10 % Copper, b) HAADF Image of Copper Particle, c) X-Ray EDS Map of Copper, d) X-Ray EDS Map of Carbon, and e) X-Ray EDS Map of Iron (scale bars for b-e are 40 nm).

[15]. Methods such as iodine doping of DWCNT cables [14] have a similar magnitude increase in conductivity (3.33X) as compared to the RES process (1.4X to 4.0X) whereas densification and doping of CNT wires with potassium tetrabromoaurate [16] and the creation of copper-CNT hybrids via site specific CVD [17] have substantially higher changes in conductivity, 13X and 569X, respectively. It is important to note that conductivity improvement of CNT wires via densification and doping requires two steps to include use of a drawing die and completion of a doping process [16]. Additionally, the copper-CNT hybrids discussed above, while demonstrating an exceptional increase in conductivity, use a substantial amount of copper (94.2 wt% Cu) [17] which

may impact their use in some weight sensitive applications. Table 2 below provides a summary of some of the conductivity increases found in literature and presented in this article.

In sum, this unique method of depositing a solution of copper salts on CNT sheets and reducing the salts through use of a reducing agent (urea), effectively bridges a metal (copper) to CNT bundles and is shown to improve electrical conductivity. SEM and TEM images in Figs. 7 and 8 clearly illustrate effective bridging between CNTs through the use of copper particles, generating what could be considered a Cu nanoparticle - CNT sheet composite or a metal – carbon hybrid structure. By dissolving copper salts in ethanol, applying this solution to CNT
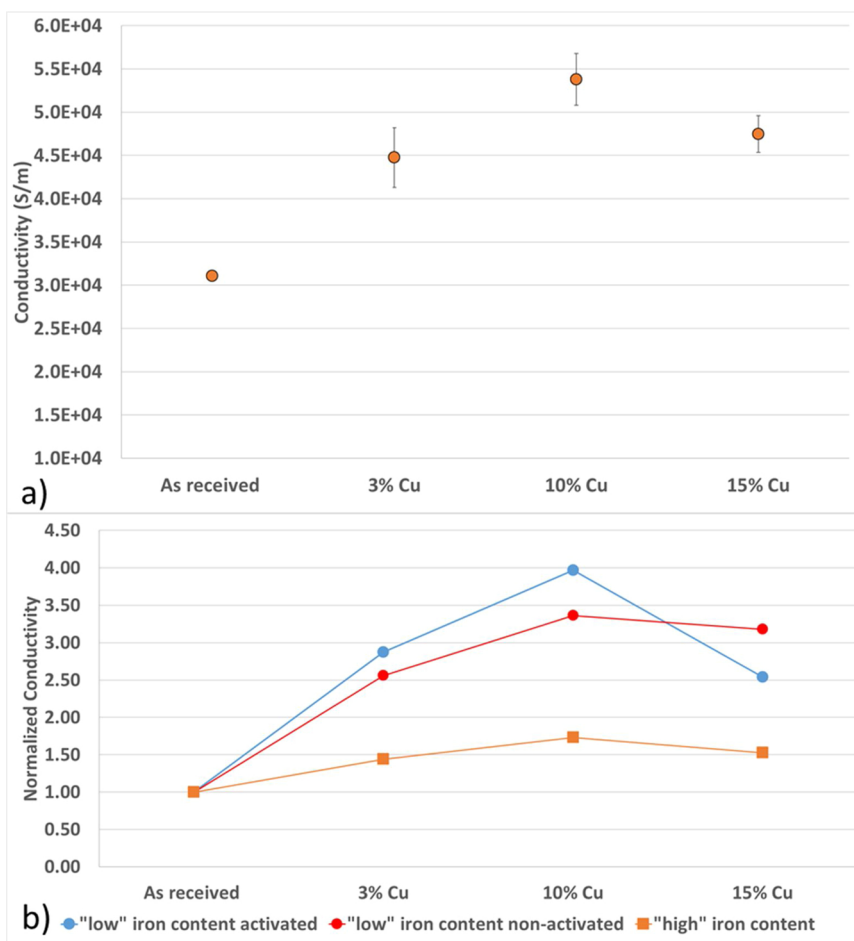
Fig. 9. a) High Fe CNT Sheet Conductivity at Varying Copper Percentages and b) Normalized Conductivity for CNT Sheets with Differing Fe Content and Activation Conditions at Varying Copper Percentages.

sheets, and then exposing the sheet to decomposing urea in a high temperature inert atmosphere, copper particles are able to be attached to CNT sheets and result in an increase in electrical conductivity. This overall process is illustrated in Fig. 11 which provides a schematic of the basic premise and goal of the RES process for metal reduction and attaching of copper particles to CNTs in the sheets.

4. Conclusions

The focus of this work was to develop a process for the addition of copper to CNT sheets as a potential means to improve electrical conductivity. CNT sheets, through a RES process, are able to be modified with copper particles to improve electrical conductivity from as-
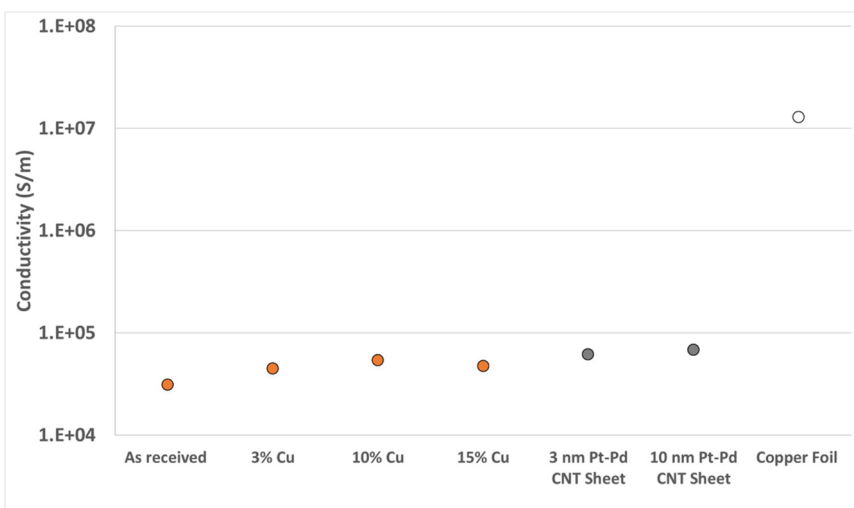

Fig. 10. Comparison of Conductivity Between CNT Sheets with Copper via RES Process, Pt-Pd Sputter Coated CNT Sheets, and Copper Foil.

Table 2

Comparison of Conductivity Improvements for Bulk CNT Materials Using Various Methods.

|	Initial Conductivity	Final Conductivity	Magnitude Increase	Reference
DWCNT Cable - Iodine Doping	$\sim 2.0 \times 10^6$ S/m	$\sim 6.7 \times 10^6$ S/m	~ 3.33X	[14]
CNT Wires - Densification and Doping with Potassium Tetrabromoaurate	$\sim 1.0 \times 10^5$ S/m	1.3×10^6 S/m	~ 13X	[16]
Copper CNT Hybrids via CVD (94.2 % wt Cu)	4.94×10^4 S/m	28.1×10^6 S/m	569X	[17]
CNT Sheets - Monobromide Doping	1.0×10^5 S/m	8.5×10^5 S/m	8.5X	[15]
CNT Yarns - Monombromide Doping	1.0×10^5 S/m	14.0×10^5 S/m	14X	[15]
RES Method (Low Fe Non-Activated) (10 % Copper)	1.0 (Relative)	3.4 (Relative)	3.4X	Current Article
RES Method (Low Fe Activated) (10 % Copper)	1.0 (Relative)	4.0 (Relative)	4.0X	Current Article
RES Method (High Fe Non-Activated) (10 % Copper)	1.0 (Relative)	1.7 (Relative)	1.7X	Current Article
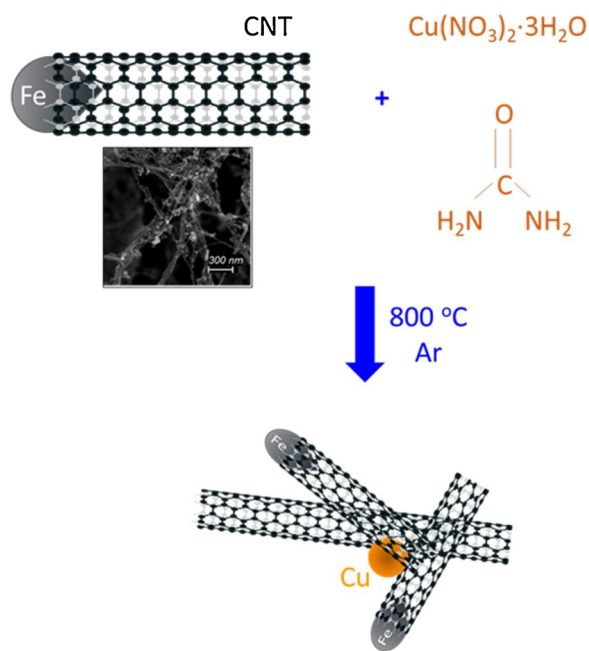
Fig. 11. RES Process Steps Leading to Addition of Copper to CNTs.

received CNT sheets by a magnitude of between 1.4X and 4.0X. The RES process presented is a scalable and cost-effective method that can be readily adapted to current processing methods. While direct doping of CNTs may prove beneficial, our proposed method has the potential to more rapidly impact electrical conductivity of manufactured CNT-sheets. By forming direct bridges between metal particles and CNTs, the RES method provides a unique means to directly attach metallic particles to CNTs that are already part of sheets and significantly improve electrical conductivity.

CRediT authorship contribution statement

Brian Earp: Investigation, Writing - original draft. **Durward Dunn:** Methodology, Investigation, Formal analysis. **Jonathan Phillips:** Writing - review & editing. **Richa Agrawal:** Investigation. **Troy Ansell:** Investigation. **Patrick Aceves:** Investigation. **Igor De Rosa:** Investigation. **Wenbo Xin:** Investigation. **Claudia Luhrs:** Conceptualization, Supervision, Project administration.

Declaration of Competing Interest

None.

Acknowledgements

Appendix A. Supplementary data

Supplementary material related to this article can be found, in the online version, at doi:https://doi.org/10.1016/j.materresbull.2020.110969.

References

[1] S. Iijima, Helical microtubules of graphitic carbon, Nature 354 (6348) (1991) 56–58.

[2] A. Lekawa-Raus, J. Patmore, L. Kurzepa, J. Bulmer, K. Koziol, Electrical properties of carbon nanotube based fibers and their future use in electrical wiring, Adv. Funct. Mater. 24 (24) (2014) 3661–3682.

[3] P.J.F. Harris, Carbon nanotube composites, Int. Mater. Rev. 49 (1) (2004) 31–43.

[4] S. Bellucci, C. Balasubramanian, F. Micciulla, G. Rinaldi, CNT composites for aerospace applications, J. Exp. Nanosci. 2 (3) (2007) 193–206.

[5] B. Earp, et al., Electrically conductive CNT composites at loadings below theoretical percolation values, Nanomaterials 9 (4) (2019) p. 491.

[6] M.F.L. De Volder, S.H. Tawfick, R.H. Baughman, A.J. Hart, Carbon nanotubes: present and future commercial applications, Science 339 (6119) (2013) 535–539.

[7] S. Zhang, J.G. Park, N. Nguyen, C. Jolowsky, A. Hao, R. Liang, Ultra-high conductivity and metallic conduction mechanism of scale-up continuous carbon nanotube sheets by mechanical stretching and stable chemical doping, Carbon 125 (2017) 649–658.

[8] Q. Cao, Q. Yu, D.W. Connell, G. Yu, Titania/carbon nanotube composite (TiO2/CNT) and its application for removal of organic pollutants, Clean Technol. Environ. Policy 15 (6) (2013) 871–880.

[9] L. Duclaux, Review of the doping of carbon nanotubes (multiwalled and single-walled), Carbon 40 (10) (2002) 1751–1764.

[10] K. Choi, C. Yu, Highly doped carbon nanotubes with gold nanoparticles and their influence on electrical conductivity and thermopower of nanocomposites, PLoS One 7 (9) (2012) p. e44977.

[11] V.Z. Mordkovich, M. Baxendale, R.P.H. Chang, S. Yoshimura, Intercalation into carbon nanotubes without breaking the tubular structure, Synth. Met. 86 (1–3) (1997) 2049–2050.

[12] P. Ayala, R. Arenal, M. Rümmeli, A. Rubio, T. Pichler, The doping of carbon nanotubes with nitrogen and their potential applications, Carbon 48 (3) (2010) 575–586.

[13] Y.K. Chen, L.V. Liu, W.Q. Tian, Y.A. Wang, Theoretical studies of transition-metal-doped single-walled carbon nanotubes, J. Phys. Chem. C 115 (19) (2011) 9306–9311.

[14] Y. Zhao, J. Wei, R. Vajtai, P.M. Ajayan, E.V. Barrera, Iodine doped carbon nanotube cables exceeding specific electrical conductivity of metals, Sci. Rep. 1 (1) (2011).

[15] A.R. Bucossi, Q. Campbell, J.E. Rossi, B.J. Landi, Effects of solution properties on iodine monobromide doping for enhanced bulk carbon nanotube electrical conductivity, ACS Appl. Nano Mater. 1 (5) (2018) 2088–2094.

[16] J. Alvarenga, et al., High conductivity carbon nanotube wires from radial densification and ionic doping, Appl. Phys. Lett. 97 (18) (2010) p. 182106.

[17] A.P. Leggiero, et al., High conductivity copper–carbon nanotube hybrids via site-specific chemical vapor deposition, Acs Appl. Nano Mater. 2 (1) (2019) 118–126.

[18] S. Wakeland, R. Martinez, J.K. Grey, C.C. Luhrs, Production of graphene from graphite oxide using urea as expansion–reduction agent, Carbon 48 (12) (2010) 3463–3470.

[19] H. Zea, C.C. Luhrs, J. Phillips, Reductive/expansion synthesis of zero valent sub-micron and nanometal particles, J. Mater. Res. 26 (5) (2011) 672–681.

[20] M. Mowry, D. Palaniuk, C.C. Luhrs, S. Osswald, In situ Raman spectroscopy and thermal analysis of the formation of nitrogen-doped graphene from urea and graphite oxide, RSC Adv. 3 (44) (2013) 21763–21775.

[21] H. Soliman, J. Phillips, C. Luhrs, H. Zea, Z.C. Leseman, Aerosol Synthesis of Nano and Micro-Scale Zero Valent Nickel Particles From Oxide Precursors, (2010), pp. 569–573.

[22] C. Luhrs, M. Kane, Z. Leseman, J. Phillips, Novel process for solid state reduction of metal oxides and hydroxides, Metall. Mater. Trans. B 44 (1) (2013) 115–122.

[23] R. Canty, E. Gonzalez, C. MacDonald, S. Osswald, H. Zea, C.C. Luhrs, Reduction expansion synthesis as strategy to control nitrogen doping level and surface area in graphene, Materials (Basel) 8 (10) (2015) 7048–7058.

[24] S.K. Menon, C.C. Luhrs, P.J. Arias-Monje, H. Zea, S. Osswald, Nitrogen Doped Graphene Generated by Microwave Plasma and Reduction Expansion Synthesis, (2016).

[25] P. Chamoli, M.K. Das, K.K. Kar, Urea-assisted low temperature green synthesis of graphene nanosheets for transparent conducting film, J. Phys. Chem. Solids 113 (2018) 17–25.

[26] P. Chamoli, M.K. Das, K.K. Kar, Structural, optical and electronic characteristics of N-doped graphene nanosheets synthesized using urea as reducing agent and nitrogen precursor, Mater. Res. Express 4 (1) (2017) p. 015012.

[27] C. Pelar, K. Greenaway, H. Zea, C.-H. Wu, C. Luhrs, J. Phillips, Novel chemical process for producing chrome coated metal, Materials 11 (1) (2018) p. 78.

[28] T.L. Lee, et al., High-stability tin/carbon battery electrodes produced using reduction expansion synthesis, Carbon 132 (2018) 411–419.

[29] L. Elbaz, J. Phillips, K. Artyushkova, K. More, E.L. Brosha, Evidence of high electrocatalytic activity of molybdenum carbide supported platinum nanorafts, J. Electrochem. Soc. 162 (9) (2015) H681–H685.

[30] N. Technologies, Nanocomp Technologies' Products | Sheet/Tape. [Online], Available: http://www.miralon.com/sheet/tape. [Accessed: 09-Jan-2019] (2020).

[31] W. Xin, J.-M. Yang, C. Li, M.S. Goorsky, L. Carlson, I.M. De Rosa, Novel strategy for one-pot synthesis of gold nanoplates on carbon nanotube sheet As an effective flexible SERS substrate, ACS Appl. Mater. Interfaces 9 (7) (2017) 6246–6254.

[32] W. Xin, et al., Graphene template-induced growth of single-crystalline gold nanobelts with high structural tunability, Nanoscale 10 (6) (2018) 2764–2773.

[33] S. Osswald, Y. Gogotsi, In situ Raman spectroscopy of oxidation of carbon nanomaterials, in: C.S.S.R. Kumar (Ed.), Raman Spectroscopy for Nanomaterials Characterization, Springer, Berlin, Heidelberg, 2012, pp. 291–351.

[34] C.C. Luhrs, D. Garcia, M. Tehrani, M. Al-Haik, M.R. Taha, J. Phillips, Generation of carbon nanofilaments on carbon fibers at 550°C, Carbon 47 (13) (2009) 3071–3078.

[35] N.L. Wu, J. Phillips, XRD evidence of preferential orientation of platinum crystallites on graphite, Surf. Sci. 184 (3) (1987) 463–482.

[36] S. Ratkovic, Dj. Vujicic, E. Kiss, G. Boskovic, O. Geszti, Different degrees of weak metal–support interaction in Fe–(Ni)/Al2O3 catalyst governing activity and selectivity in carbon nanotubes' production using ethylene, Mater. Chem. Phys. 129 (1) (2011) 398–405.

[37] M.V. Smoluchowski, Drei Vortrage uber diffusion, Brownsche Bewegung und Koagulation von Kolloidteilchen, Zeitschrift Fur Physik 17 (1916) 557–585.

[38] N. Albertovič. Fuks, The Mechanics of Aerosols, Dover Publications, New York, 1964.

[39] M. Frenklach, Method of moments with interpolative closure, Chem. Eng. Sci. 57 (12) (2002) 2229–2239.

[40] M. Frenklach, J.P. Hsu, D.L. Miller, R.A. Matula, Shock-tube pyrolysis of chlorinated hydrocarbons: formation of soot, Combust. Flame 64 (2) (1986) 141–155.

[41] D.W. Clary, Soot Formation During Pyrolysis of Aromatic Hydrocarbons (Modeling, Shock-Tube, Acetylene, Butadiene), (2020) p. 324.

[42] P. Savi, M. Giorcelli, S. Quaranta, Multi-walled carbon nanotubes composites for microwave absorbing applications, Appl. Sci. 9 (5) (2019) p. 851.

[43] B. Adeniran, R. Mokaya, Low temperature synthesized carbon nanotube superstructures with superior CO_2 and hydrogen storage capacity, J. Mater. Chem. A 3 (9) (2015) 5148–5161.

[44] Article Chemical Engineering July 2017 Activated Carbon Fundamentals and New Applications | Adsorption | Biogas, Scribd, 2020 [Online]. Available: https://www.scribd.com/document/374438144/Article-Chemical-Engineering-July-2017-Activated-Carbon-Fundamentals-and-New-Applications. [Accessed: 17-Sep-2019].

[45] L.M. Ang, T.S.A. Hor, G.Q. Xu, C.H. Tung, S.P. Zhao, J.L.S. Wang, Decoration of activated carbon nanotubes with copper and nickel, Carbon 38 (3) (2000) 363–372.